IL NUOVO CIMENTO Vol. 31 C, N. 3 Maggio-Giugno 2008
DOI 10.1393/ncc/i2008-10297-1

Archaeometric investigation of red-figure pottery fragments from Gioiosa Guardia (Messina, Sicily) by INAA, FT-IR and TOF-ND techniques

D. Barilaro([1]), V. Crupi([1]), S. Interdonato([1]), F. Longo([1]), G. Maisano([1]), D. Majolino([1])(*), V. Venuti([1]), G. Barone([2]), P. Mazzoleni([2]), G. Tigano([3]), S. Imberti([4]) and W. Kockelmann([5])

([1]) *Dipartimento di Fisica, Università di Messina and CNISM, UdR Messina - C.da Papardo S.ta Sperone 31, 98166 Messina, Italy*
([2]) *Dipartimento di Scienze Geologiche, Università di Catania - Corso Italia 57 95129 Catania, Italy*
([3]) *Soprintendenza Beni Culturali ed Ambientali di Messina, Sezione Archeologica Viale Boccetta 38, 98100, Messina, Italy*
([4]) *CNR, Istituto Sistemi Complessi: Sezione di Firenze - Via Madonna del Piano 10 50019 Sesto Fiorentino, Italy*
([5]) *ISIS Facility, Rutherford Appleton Laboratory - Didcot, OX11 0QX, UK*

(ricevuto il 4 Settembre 2008; revisionato il 3 Dicembre 2008; approvato il 3 Dicembre 2008; pubblicato online il 13 Gennaio 2009)

Summary. — The present work is addressed to the study of some precious ancient pottery fragments, coming from the archaeological site of Gioiosa Guardia, in the Tirrenean Coast of Sicily. On the basis of historical and aesthetic considerations, the findings are dated back to VI-V century b. C. and show a surface entirely decorated by red-figure technique, typical of Attic production. Many doubts arise about the real provenance of the artefacts. On one side, they could come directly from Greece, as attested by trading patterns between Greece and Southern Italy, on the other side, they could be produced in Sicily under the Greek artistic influence. In order to obtain a detailed characterization of the samples, a microdistructive investigation was performed by Instrumental Neutron Activation Analysis (INAA), Fourier transform infrared absorption (FT-IR) and a non-invasive analysis by time-of-flight neutron diffraction (TOF-ND). Starting from the identification of the mineralogical and geochemical composition, a correct classification of the shards can be achieved.

PACS 29.30.Hs – Neutron spectroscopy.
PACS 33.20.Ea – Infrared spectra.
PACS 81.05.Je – Ceramics and refractories (including borides, carbides, hydrides, nitrides, oxides, and silicides).

(*) E-mail: majolino@unime.it

1. – Introduction

Potteries, present from ancient times and typical product of the culture of every single people, represent the richest of data testimony of the ancient world. In addition, they associate to the richness of historical information an interesting physical complexity due to the coexistence, in the same sample, of amorphous and crystalline phases.

Scientific examination of pottery is one of the oldest fields in archaeometry. Studies on these findings allowed to get chemical-physical information such as the composition in terms of element and minerals [1-7], mesoscopic structures [7, 8], up to macroscopic inhomogeneities [9-12]. This information is very precious for the dating of the artefact, for the individuation of its provenance or authenticity and for the characterization of the manufacture technique, and hence, in principle, for the reconstruction of the commercial and cultural exchanges among populations.

Obviously, the search for non-invasive or, at least, microdestructive techniques is of paramount importance when dealing with objects of great historic, cultural and artistic value, in order to eliminate cutting, coring or drilling of the finding involved in a sampling procedure or to reduce the amount of extracted material to a minimum.

The high-penetration capability of neutrons makes neutron methods ideal non-destructive tools for archaeometric investigations [13]. In addition, the exposure of a considerable volume portion of the object in the beam allows for an averaged and statistically meaningful structural information, representative of the bulk of the entire artefact.

Neutron beam has been frequently used as a probe for archaeometric research in high-sensitivity element specific prompt gamma activation analysis for provenance studies [14], whereas neutron radiography provides a high-resolution inside view of intact and bulky objects [15, 16].

Some years ago, systematic archaeometric studies for the characterization of archaeological findings by neutron diffraction started and grew up very rapidly [17-21]. Quantitative information on mineral and metal phases composition, crystal structure parameters of each phase, grain sizes and orientations can be obtained. Texture analysis can be performed, in order to go deep into the thermal treatment of the sample, gaining details of its production steps [22-26].

In this framework, we present here the results of the joint employment of microdesctructive techniques such as Instrumental Neutron Activation Analysis (INAA) and Fourier transform infrared absorption (FT-IR), and non-destructive such as time-of-flight neutron diffraction (TOF-ND), for the characterization of some precious ancient pottery shards coming from Gioiosa Guardia (Sicily, Southern Italy).

The archaeological site of Gioiosa Guardia, in the Tirrenean Coast of Sicily between Capo Calavà and Capo d'Orlando (see fig. 1), discovered in 80s and only partially explored, revealed a habitative continuity from prehistoric to classical age [27, 28]. The excavations brought to light a wide part of the Greek built-up area lying on the rests of two previous settlements dated back to the ancient Bronze and Iron Ages. In the site, a big variety of artefacts can be recognized, mainly belonging to the most recent habitative period (VI–V century b. C.). The findings coming from this archeological site have not been studied up to now from the archaeometric point of view and, in addition, no historical fonts exist concerning the period these potteries belong to. We focused our attention on four red-figure pottery fragments that exhibit similar macroscopic characteristics.

The main task of the study is, first of all, to verify if samples are also comparable from the microscopic point of view and, starting from their microscopic structure, to identify the production areas and to get information on the firing temperatures. The

Fig. 1. – Map of Gioiosa Guardia (Province of Messina, Sicily, Southern Italy).

extracted information will be very useful in order to reconstruct the economical and cultural exchange patterns between this "anonymous" centre and the other Greek centres of the Coast, and to hypothesize the technological level of this specific community.

2. – Experimental

2˙1. *Samples*. – The investigated samples, labelled GI-27, GI-28, GI-29 and GI-30, were red-figure pottery fragments, belonging to a set of shards excavated from the aforementioned Gioiosa Guardia site, dated back to VI-V century b. C. As an example, the photos of the fragments GI-27 and GI-28 are shown in fig. 2 (a) and (b), respectively.

The *Soprintendenza per i Beni Culturali ed Ambientali di Messina* (the Local Government in Charge for Cultural Heritage) requested, within an established collaboration, the characterization and authentication of the fragments as a prerequisite for their cataloguing.

The macroscopic investigation allowed us to point out the most important features relevant to the "granulometry", the presence or not of inclusions in the ceramic body and the colour, described according to MUNSELL Soil Colour Chart. The results are reported in table I.

2˙2. *INAA measurements*. – Instrumental Neutron Activation Analysis [29] is a microdestructive trace element technique, capable of measuring up to 35 elements at the ppb to percent level in most materials. INAA is dependent on measuring primary gamma radiation which is emitted by the radioactive isotopes produced by irradiating samples in a nuclear reactor. Each element which is activated will emit a "fingerprint" of gamma radiation which can be measured and quantified.

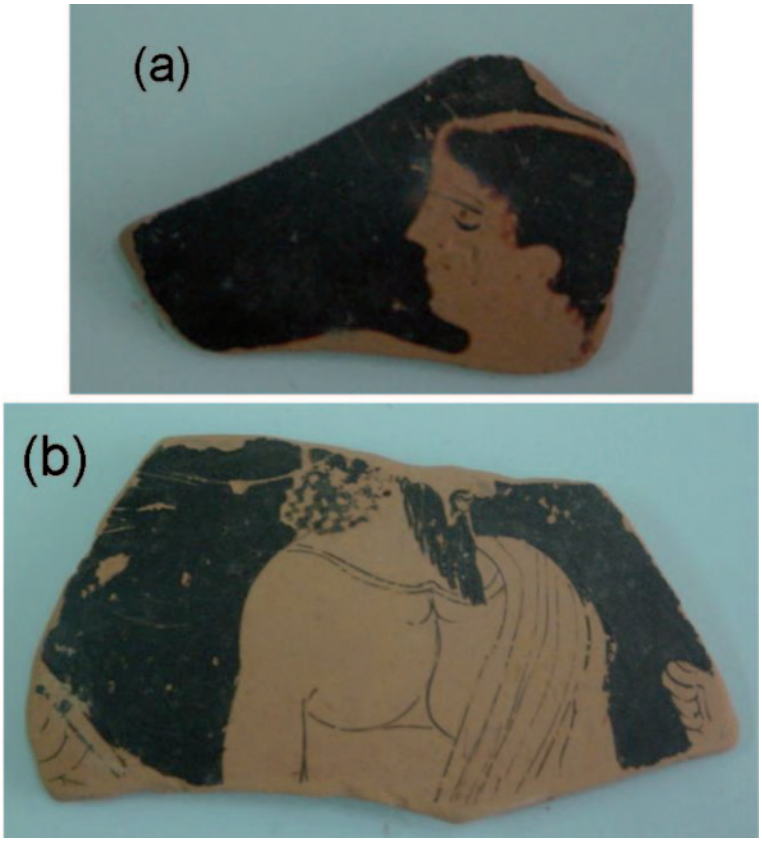

Fig. 2. – Pictures of sample GI-27 (a) and GI-28 (b).

As it requires no chemistry, there is little worry of contamination or whether the elements in question are in solution. The additional worry of whether there are abnormal amounts of a particular element which will cause chemical or instrumental interferences is also generally avoided with INAA. INAA is exceptionally sensitive to a number of trace elements (gold, arsenic, antimony, tantalum, uranium, thorium, etc.), many of them very difficult and expensive to determine by conventional chemical procedures. The INAA technique does not require the expensive and slow ashing procedure of other chemical methods. This lack of ashing prevents potential loss of certain elements and improves the reliability of data due to lesser sample handling and potential human error.

INAA measurements have been performed by a contract analytical service furnished by the Actlabs (Activation Laboratories Ltd.) Group of Companies in Ancaster, Ontario.

The 4A-Research-INAA code was used, whose detailed description is reported in the `www.actlabsint.com` web site.

2˙3. *FT-IR measurements.* – FT-IR analysis was carried out by using a BOMEM DA8 FTIR spectrometer. The experimental set-up was equipped with a Globar lamp source, a KBr beamsplitter and a DTGS/MIR detector, that spanned a spectral range from 450 to 4000 cm^{-1}. In such a configuration it was possible to use a resolution of 4 cm^{-1}. The investigated samples were prepared in pellets, about 0.5 mm thick, using small quantities

TABLE I. – *Macroscopic description of all the analysed fragments.*

Sample	Granulometry	Colour (MUNSELL Soil Colour Chart)	Inclusions (frequency, colour and dimension)	Voids (frequency and dimension)	Surface	Thickness (cm)
GI-27	fine	2.5YR 7/6 (light red)	absent	very rare $\varnothing < 1$ mm	smooth	0.6
GI-28	fine	Varying from 2.5YR 8/2 (pinkish white) to 2.5YR 7/3 (light reddish brown)	absent	very rare $\varnothing < 1$ mm	smooth	0.6
GI-29	fine	2.5YR 8/3 (pink)	absent	very rare $\varnothing < 1$ mm	smooth	0.7
GI-30	fine	2.5YR 8/4 (pink) with edge 2.5YR 5/6 (red)	absent	very rare $\varnothing < 1$ mm	smooth	0.3

(~ 2 mg) of bulk sample dispersed in ~ 200 mg of powdered CsI, that is transparent in the investigated frequency range. The measurements were performed in dry atmosphere to avoid dirty contributions. 32 repetitive scans were automatically added to obtain a good signal-to-noise ratio (SNR) and a spectra reproducibility of high quality as well. The experimental IR spectra were compared with Sadtler database [30] ("Mineral and Clays") in order to interpret the spectral features. We remark that, even if a sampling is necessary, the quantity of powdered sample required for the measurement is just 2 mg, so the requirement of micro-destructivity is fulfilled.

2˙4. *TOF-ND measurements.* – From a general point of view, in a powder diffraction experiment the resulting pattern of diffraction peaks is a fingerprint characteristic for the whole assembly of crystalline phases in the sample, in the form of scattered intensity *vs.* diffraction angle (angle-dispersive mode) or scattered intensity *vs.* diffraction energy (energy-dispersive mode) [31].

In both cases, the interaction is formalized by Bragg's law:

$$\lambda = 2d_{hkl} \sin\theta, \tag{1}$$

where the incident neutron wavelength λ is comparable with the lattice plane spacing d_{hkl} of a mineral.

Measuring in the angle-dispersive mode, the wavelength λ is maintained constant using monochromatic radiation, and diffraction peaks are obtained at varying scattering angles 2θ, depending on the distribution of the distances d_{hkl} between the crystallographic planes. On the other side, in the energy-dispersive mode, that we used in our measurements, the incident neutron energy is varied and discriminated by measuring the

TABLE II. – *Instrumental parameters of INES diffractometer.*

Wavelength	0.17–3.24 Å
Incident flight path	22.804 m
Scattered flight path	1 m
Angular range	11.6°–170.6°
Q range	0.4–60 $Å^{-1}$
d range	0.1–16 Å
Beam size	$40 \times 40\,mm^2$

neutron flight time t = TOF on a distance L from source to detector. The scattered intensity, measured at a fixed angle 2θ, will exhibit diffraction peaks as a function of neutron energy or wavelength. Using the de Broglie relationship it is easy to connect t to the d_{hkl}-spacing:

$$t = 505.56 L d_{hkl} \sin\theta. \tag{2}$$

We carried out the neutron diffraction (ND) measurements on samples GI-27, GI-29 and GI-30 by the time-of-flight (TOF) diffractometer INES installed at the neutron spallation source ISIS (Rutherfored Appleton Laboratory, UK) having one of the main applications in the field of archaeometry, for a highly reliable determination of composition of ceramics. Its wide sample tank (diameter = 80 cm) allows the measurement of bulky archaeological artefacts without any prior preparation, so in a non-destructive way. The layout of this instrument is reported in table II.

Static measurement configurations and relatively long acquisition times (6-7 h) were used for phase analysis. The refinement of the phase weight fractions and/or structure parameters from the acquired d-spacing spectra were achieved using the public-domain program suite GSAS [32], by following the well-established quantitative multi-bank Rietveld analysis [33].

3. – Results and discussion

3˙1. *INAA data.* – In table III we report the INAA data obtained for the analysed pottery fragments.

Samples GI-27 and GI-30 show similar contents of Cr, Ni, As, Ce, Co, La, Na, Sb and Th. Furthermore, they differ from samples GI-28 and GI-29 for the higher contents of Ni, Cr, As, Co and Sb, and lower contents of La, Ce, Na e Th.

As can be seen, the most significant result is represented by the tenors in Cr and Ni that turn out to be definitively higher for GI-27 and GI-30 findings with respect to GI-28 and GI-29. This occurrence allowed us to get important information concerning the provenance area of the samples under study. As is shown in the Cr *vs.* Ni variation plot (fig. 3), the concentrations of these two elements for GI-27 and GI-30 belong to the compositional field of the ceramics of Greek production [34], whereas GI-28 and GI-29, exhibiting notably lower tenors indicating a Western production [34] with amounts similar to those of some ceramics of the Strait area.

TABLE III. – *INAA results for all the analysed fragments (the data are all expressed in ppm, with the exception of* Ca *and* Fe *that are expressed in %).*

Element	GI-27	GI-28	GI-29	GI-30	Det. Lim.
Cr	544	275	165	595	0.50
As	70	54	18	93	1.00
Ba	540	600	580	730	50.0
Ca	3.3	3.9	6.6	3	0.20
Ce	71	95	100	80	1.00
Co	42	25	28	44	0.50
Cs	4.1	3.6	3.5	5.5	0.50
Eu	< 0.05	2	1.6	1.8	0.05
Fe	6.21	5.59	6.46	6.66	0.01
Hf	3	5	3	4	0.20
La	35.6	48.6	50	39.8	0.10
Lu	0.44	0.52	0.46	0.5	0.01
Na	4000	8690	7580	4600	50.0
Nd	92	91	120	77	3.00
Ni	380	< 50	< 50	390	50.0
Rb	70	80	90	80	10.0
Sb	1.9	1.1	0.7	2	0.10
Sc	22.2	22.1	21.9	25.8	0.01
Sm	6.92	8.6	7.99	7.77	0.01
Th	13	17	18	13	0.20
Yb	3.2	3.7	3.2	3.4	0.05
Zn	320	320	390	280	20.0

3˙2. *FT-IR data.* – All the four samples were investigated by FT-IR absorbance spectroscopy. The recorded spectra were deconvoluted by a best-fit procedure in order to achieve, by a comparison with standard data, a reliable assignment of each band to the corresponding compound and then to obtain the identification of the mineralogical phases in the pottery. The findings were investigated both in the inner bulk (samples labelled as GI-27 int, GI-28 int, GI-29 int, GI-30 int) and on the surface layer (samples labelled as GI-27 ext, GI-28 ext, GI-29 ext, GI-30 ext). In particular, the external layer was analysed in order to tentatively identify the colouring agents used for the artistic decorations. Figure 4 shows a typical example of FT-IR spectrum as obtained, in all the investigated range, for the inner bulk and the external layer of GI-29 sample.

Figures 5 and 6 report for the inner and external part of GI-27 and GI-28 samples respectively, as examples, the results of the best fit performed on the experimental FT-IR

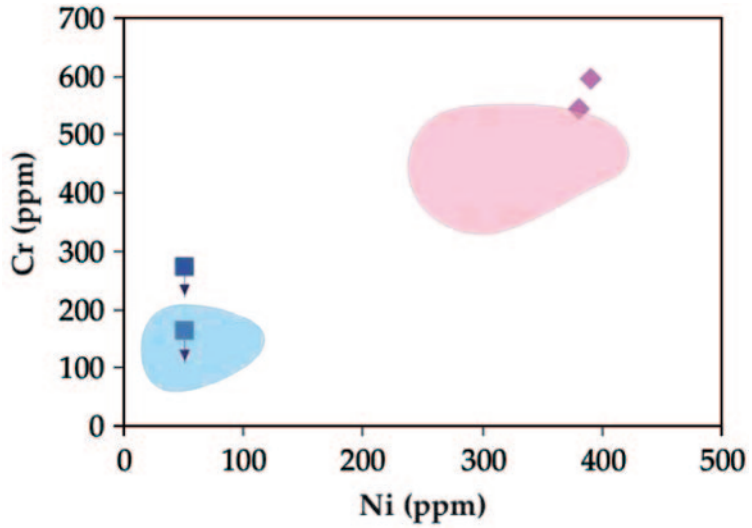

Fig. 3. – Ni *vs.* Cr variation plot for all the analysed fragments (squares: GI-28 and GI-29, diamonds: GI-27 and GI-30), as obtained by INAA measurements, together with the areas in which the reference data are confined (blue area: Western production, pink area: Greek production).

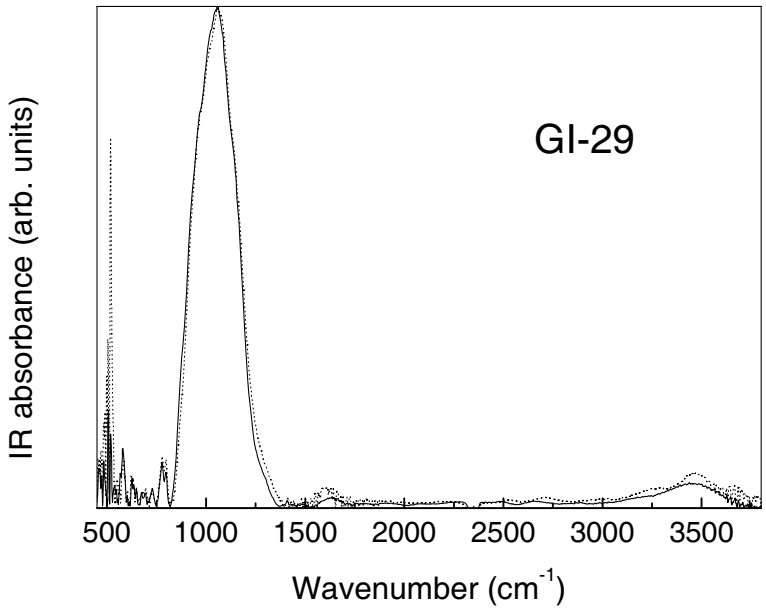

Fig. 4. – FT-IR spectra in the 450–3800 cm^{-1} range for the inner bulk (solid line) and the external layer (dotted line) of GI-29 sample.

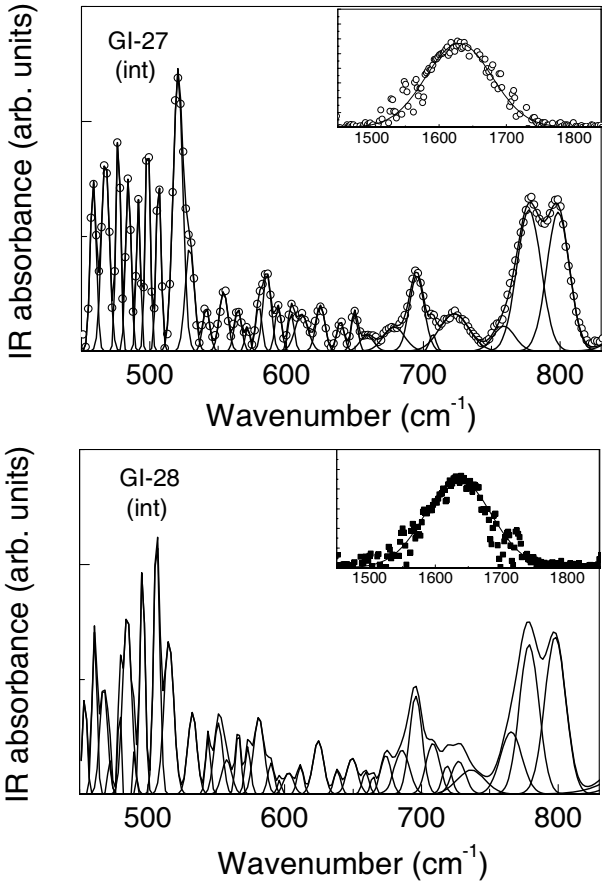

Fig. 5. – FT-IR spectra in the 450–850 cm^{-1} range for the inner bulk of GI-27 (top) and GI-28 (bottom) samples, together with the theoretical fit (continuous line) and the deconvolution components (dashed lines). In the inset of each figure, the best-fit results for the 1450–1850 cm^{-1} range are shown.

spectra in the most significant frequency ranges from 450 to 850 cm^{-1} and from 1450 to 2000 cm^{-1}. Indeed, in the range from 850 to 1450 cm^{-1} in order to avoid an overinterpretation of the data, the large band has been not fitted.

The wave-numbers of the single components, obtained as best-fit parameters, were assigned by a comparison with the typical wave-numbers of the contributions to the FT-IR spectra of minerals given in the Sadtler database "Mineral and Clays" [30], and allowed us to distinguish, as main components of the pottery findings, quartz, feldspar, plagioclase, diopside, wollastonite, clay and iron oxides. They are reported in tables IV and V for the inner bulk and the external layer of all the investigated samples, respectively. In addition, minerals within the same class exhibit a similar spectrum but with some differences in the frequencies of their characteristic peaks, so a further distinction has been achieved. The feldspar minerals present in the ceramic paste were revealed to be orthoclase and microcline. As far as plagioclases are concerned, they seem to be mainly of bytownitic nature.

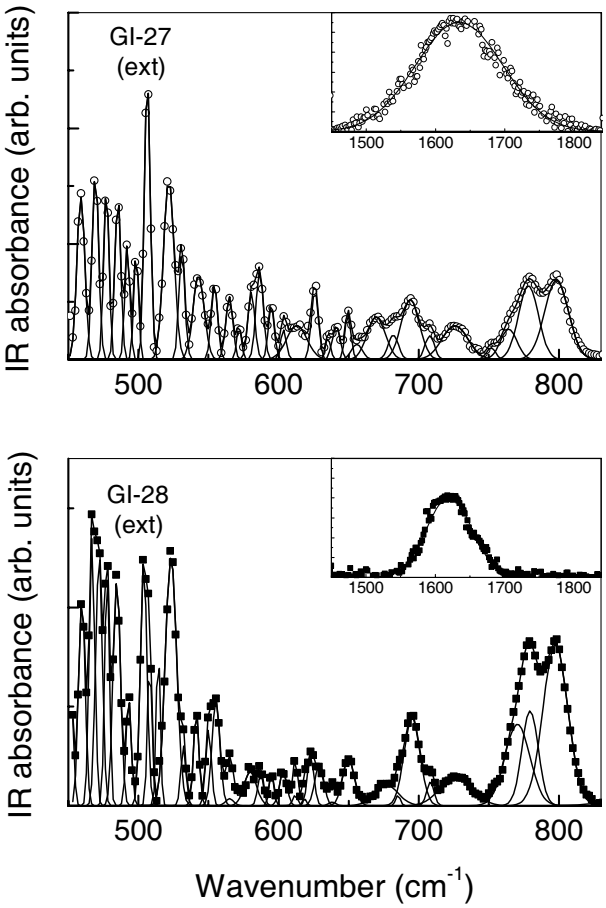

Fig. 6. – FT-IR spectra in the 450–850 cm^{-1} range for the external layer of GI-27 (top) and GI-28 (bottom) samples, together with the theoretical fit (continuous line) and the deconvolution components (dashed lines). In the inset of each figure, the best-fit results for the 1450–1850 cm^{-1} range are shown.

Again, diopside and/or wollastonite are detected in all the analysed samples. The identification of these two neo-formation minerals attests a firing temperature higher than 900 °C because, as is well known [35, 36], they originate from chemical reactions between quartz and carbonates occurring at 900 °C. Then, this evidence is strictly related to the firing process of the ceramics and gives information about the manufacture technology of the pottery. As far as the clay materials are concerned, the presence of both illite and montmorillonite can be assumed. Montmorillonite usually fades away for temperatures higher than 200 °C, but the hypothesis of such a low firing temperature contrasts with the wide and attested documentation about the pottery manufacture. Montmorillonite could derive from hydrolysis processes occurring during the burial period of the findings.

Even if the mineralogical composition of the samples appears rather uniform, the characterization obtained by FT-IR data allowed us to get similarities in the obtained wave-numbers between GI-27 and GI-30 (for both the inner bulk and the external layer) and between GI-28 and GI-29 shards. Then, in agreement with INAA results, two sub-

TABLE IV. – *Band components FT-IR wave-number revealed for the inner bulk of all the analysed samples by the curve fitting procedure and their assignment (for each wave-number, we indicated in brackets other contributions the peak is convoluted with: quartz = Qz, orthoclase = Or, Microcline = Mi, bytownite = Bw, diopside = Di, wollastonite = Wo, illite = Il, montmorillonite = Mont, iron oxides = Ir Ox).*

Assignment		GI-27 int	GI-28 int	GI-29 int	GI-30 int
Quartz		458.7 (Or) 506.5 (Di) 695.2 778.4 797.8	461.0 (Or) 506.4 (Di) 695.9 778.8 797.8	460.7 (Or) 506.5 (Di) 695.3 778.4 797.6	457.9 (Or) 505.8 (Di) 695.0 778.1 797.9
Feldspar	Orthoclase	458.7 (Qz) 528.9 (Mi) 579.3 (Bw) 639.4 (Mi, Wo) 722.6 (Mi)	461.0 (Qz) 532.4 (Mi) 581.0 (Bw) 638.3 (Mi, Wo) 718.8 (Mi)	460.7 (Qz) - 581.1 (Bw) 636.9 (Mi, Wo) 727.7 (Mi)	457.9 (Qz) 529.4 (Mi) 578.3 (Bw) 637.6 (Mi, Wo) 725.9 (Mi)
	Microcline	476.9 484.3 528.9 (Or) - 639.4 (Or, Wo) 722.6 (Or) 766.2	479.3 484.8 532.4 (Or) 573.0 638.3 (Or, Wo) 718.8 (Or) 765.6	479.1 484.9 - 573.6 636.9 (Or, Wo) 727.7 (Or) 764.3	477.2 484.6 - 529.4 (Or) 637.6 (Or, Wo) 725.9 (Or) 768.1
Plagioclase	Bytownite	541.2 579.3 (Or) 624.7 (Di) -	- 581.0 (Or) 624.6 (Di) 736.4	543.2 581.1 (Or) 625.8 (Di) 736.0	540.5 578.3 (Or) 625.1 (Di) -
Diopside		506.5 (Qz) 624.7 (Bw) -	506.4 (Qz) 624.6 (Bw) 664.7	506.5 (Qz) 625.8 (Bw) 664.6	505.8 (Qz) 625.1 (Bw) -
Wollastonite		564.4 639.4 (Or, Mi) 678.8	566.1 638.3 (Or, Mi) 673.9	560.2 636.9 (Or, Mi) 673.8	564.4 637.6 (Or, Mi) 677.9
Clay	Illite	1629.5 3200–3600 range (Mont)	1634.8 3200–3600 range (Mont)	1634.8 3200–3600 range (Mont)	1643.8 3200–3600 range (Mont)
	Montmorillonite	467.6 (Ir Ox) 520.6 610.9 3200–3600 range (Il)	467.7 515.4 611.4 3200–3600 range (Il)	467.7 (Ir Ox) 518.8 611.6 3200–3600 range (Il)	469.1 (Ir Ox) 520.2 611.4 3200–3600 range (Il)
Iron Oxides		467.6 (Mont) 553.8	467.7 (Mont) 557.5	467.7 (Mont) 550.3	469.1 (Mont) 553.3

TABLE V. – *The same as table* IV *but for the external layer.*

Assignment		GI-27 ext	GI-28 ext	GI-29 ext	GI-30 ext
Quartz		458.9 (Or) 506.4 (Di) 693.9 778.2 798.2	459.6 (Or) 508.1 (Di) 695.1 779.4 797.4	459.8 (Or) 506.3 (Di) 693.8 780.0 797.3	460.8 (Or) 505.8 (Di) 694.7 777.8 798.1
Feldspar	Orthoclase	458.9 (Qz) 531.0 (M) 580.5 (Bw) 641.1 (Mi, Wo) 725.7 (Mi)	459.6 (Qz) 532.1 (Mi) 579.7 (Bw) 638.1 (Mi, Wo) 726.8 (Mi)	459.8 (Qz) - 586.0 (Bw) 635.2 (Mi, Wo) 728.6 (Mi)	460.8 (Qz) 533.0 (Mi) 579.4 (Bw) 640.7 (Mi, Wo) 726.3 (Mi)
	Microcline	477.1 - 531.0 (Or) 573.8 641.1 (Or, Wo) 725.7 (Or) 764.1	477.6 484.5 532.1 (Or) - 638.1 (Or, Wo) 726.8 (Or) 770.3	- 484.6 - 573.8 635.2 (Or, Wo) 728.6 (Or) 768.7	477.1 - 533.0 (Or) 575.7 640.7 (Or, Wo) 726.3 (Or) 765.5
Plagioclase	Bytownite	542.9 580.5 (Or) 625.9 (Di)	541.2 579.7 (Or) 622.8 (Di)	543.4 586.0 (Or) 623.0 (Di)	579.4 (Or) 624.7 (Di)
Diopside		506.4 (Qz) 625.9 (Bw) 669.6	508.1 (Qz) 622.8 (Bw) -	506.3 (Qz) 623.0 (Bw) -	505.8 (Qz) 624.7 (Bw) 668.0
Wollastonite		- 641.1 (Or, Mi) 681.8	564.9 638.1 (Or, Mi) 676.8	563.1 635.2 (Or, Mi) 674.6	- 640.7 (Or, Mi) 682.4
Clay	Illite	1634.3 3200–3600 range (Mont)	1620.3 3200–3600 range (Mont)	1614.5 3200–3600 range (Mont)	1637.0 3200–3600 range (Mont)
	Montmorillonite	469.3 (Ir Ox) 521.6 612.9 3200–3600 range (Il)	466.8 (Ir Ox) 523.2 611.8 3200–3600 range (Il)	466.6 (Ir Ox) 519.6 610.2 3200–3600 range (Il)	467.8 (Ir Ox) 520.4 610.4 3200–3600 range (Il)
Iron Oxides		469.3 (Mont) 554.2	466.8 (Mont) 555.2	466.6 (Mont) 554.4	467.8 (Mont) 551.2

groups can be recognized, suggesting, for each of them, different regions of the original materials.

The presence of iron oxides is indicative for the deep red colour of the ceramic body and the red figures decoration. In particular, the presence of a higher amount of iron oxides on the surface layer of our samples could indicate that the colouring raw material could be a ferruginous clay that, during the three stages the firing process consists of oxidizing, reducing and final re-oxidation, gives to the artefact the typical red and black colour.

This result validates, for all the analyzed samples, the application of the typical Greek red-figures decoration process. Nevertheless, it is not sufficient to attribute the shards to an original Greek production. In fact, being Sicily a flourishing Magna Graecia region, and the Tyrrhenian-Ionic coast particularly, a deep Hellenic influence in local artistic manufacture is highly presumable.

3˙3. *TOF-ND data.* – The measured diffraction patterns of the selected samples GI-29 and GI-30 are reported in figs. 7 and 8, along with the calculated fitting profile (solid line) as obtained with the Rietveld analysis, and residuals (bottom curves). As example, we show three diffraction patterns among the forward and backscattering directions of the nine groups of detectors installed on INES facility. The detector group 3 (figs. 7(a) and 8(a)) is centred at about $2\vartheta = 134.6°$ ($d_{\min} = 0.11\,\text{Å}$ and $d_{\max} = 1.76\,\text{Å}$), the detector group 5 (figs. 7(b) and 8(b)) is centred at about $2\vartheta = 98.6°$ ($d_{\min} = 0.13\,\text{Å}$ and $d_{\max} = 2.14\,\text{Å}$), and, finally, the detector group 7 (figs. 7(c) and 8(c)) is centred at about $2\vartheta = 62.6°$ ($d_{\min} = 0.19\,\text{Å}$ and $d_{\max} = 3.13\,\text{Å}$). Starting from the qualitative phase analysis obtained by FT-IR measurements, initial modelling of the observed ND data during the refinement process was based on the presence of quartz (Qz), orthoclase (Or), bytownite (Bw), haematite (Hm), spinel (Sp), diopside (Di), as mineral phases. Then, calcite (Cc), gehlenite (Gh) and illite/muscovite (Il/Mu) were also added. Each sample was firstly individually fitted with a number of phases. Afterwards, a group of phases common to all samples was identified, due to the high homogeneity of the set of findings, and the samples were fitted with this common set of phases. Free parameters were phase fractions, d-spacing zero shift, Debye-Waller factor except for muscovite for which it was fixed at the high value of $0.8\,\text{Å}^2$. The structural parameters of the starting phases were taken from the Inorganic Crystal Structure Database [37]. Unfortunately, the lack of a reliable structure model for illite/muscovite prevents the weight fraction of this mineral to be estimated, although its presence is clearly indicated by the appearance of its characteristic Bragg peaks. As the Rietveld refinement is based on a relative determination of the phases amounts, that consequently is strongly related to the number of the minerals included in the fit procedure, we choose to keep out illite/muscovite from the weight fractions computation. All the other mineral weight fractions have been renormalized to one. Table VI contains the obtained refined weight fractions as well as the goodness-of-fit parameter R_{wp} that denotes the Rietveld profile R value (in percent). For a more direct visualization, they are also reported in fig. 9. Realistic estimates of the uncertainties on the weight fraction values are about 0.5% for all investigated samples. This means that all those mineral phases whose weight fraction is below this value have to be considered as not present in the pottery. In the figures, the bar codes represent the theoretical peak positions of the mineral phases included in the fitting procedure (from Qz to Gh going from bottom to top). We remark that the Rietveld analysis has been performed on the nine simultaneously collected data sets from the nine independent detector groups with phase fractions as free parameters.

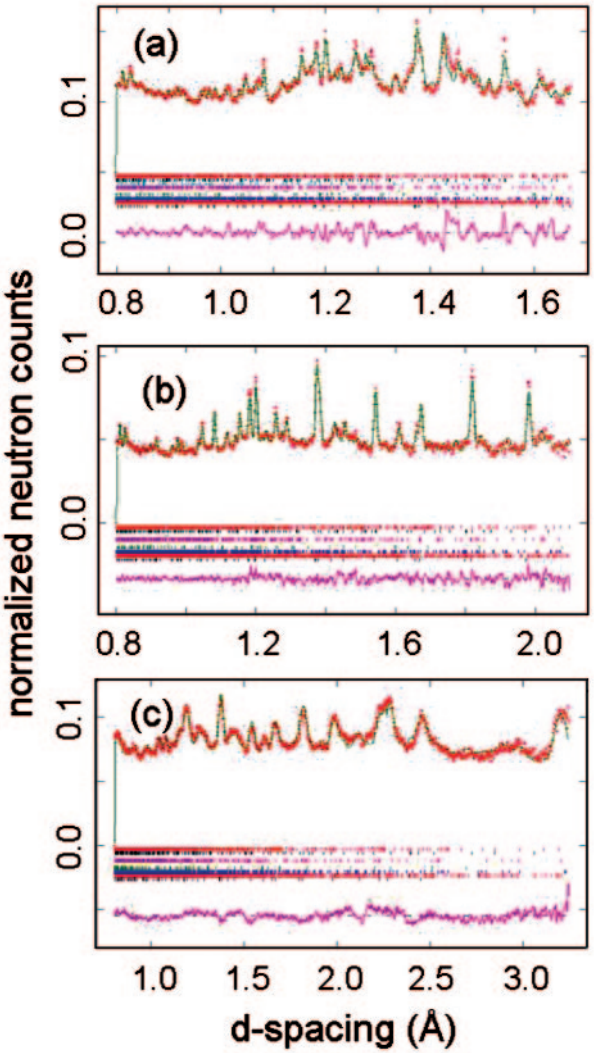

Fig. 7. – TOF backscattering (a, b) and forward (c) neutron diffraction patterns for GI-29 sample.

The composition of the samples appears to be similar, except for the absence of calcite in fragment GI-30. Even if this is not a surprising result, since all the considered minerals are typical components of pottery, the great advantage offered by neutron diffraction is to allow a complete and accurate identification of all the mineral phases in a totally non-destructive way. The complete identification of the mineral phases allows to go deeper inside the manufacture technique. In particular, gehlenite detection can provide further information about the firing temperature. In fact, since gehlenite disappears at a temperature around 900 °C, when diopside forms, the contemporary presence of these two minerals could suggest a firing temperature ranging from $\sim 900\,^{\circ}\mathrm{C}$ to $\sim 950\,^{\circ}\mathrm{C}$.

From a deep inspection of the ND data, we observe that the quantities of quartz, bytownite, haematite and spinel are comparable for GI-27 and GI-30, in contrast with

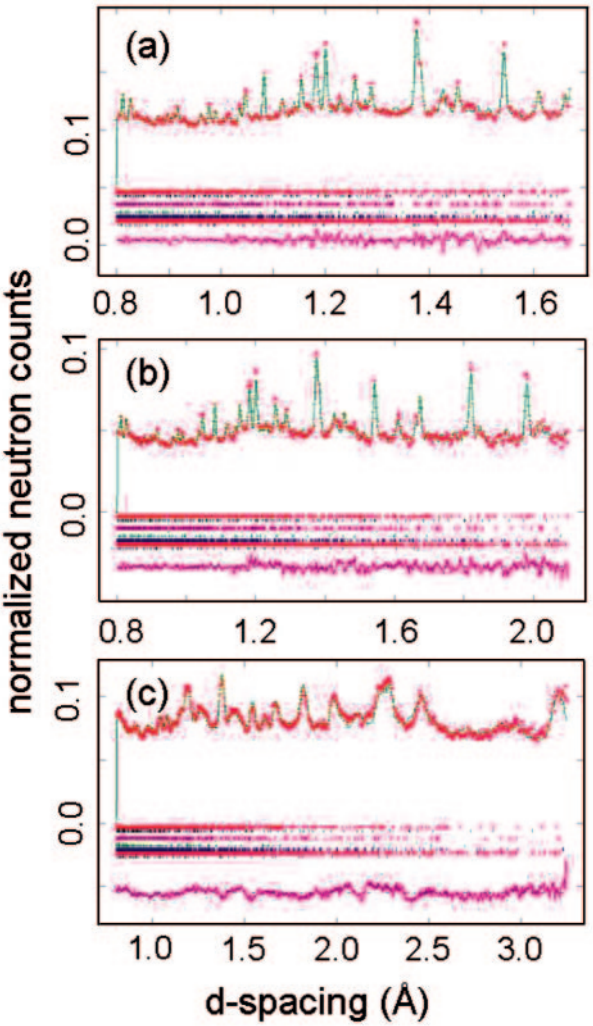

Fig. 8. – TOF backscattering (a, b) and forward (c) neutron diffraction patterns for GI-30 sample.

TABLE VI. – *Refined weight fractions, as obtained from Rietveld analysis, together with goodness-of-fit parameters* χ^2 *and* R_{wp}.

Sample	Qz	Or	Bw	Hm	Sp	Di	Cc	Gh	χ^2	R_{wp}
GI-27	0.436	0.146	0.208	0.043	0.027	0.091	0.014	0.035	3.462	3.06
GI-29	0.152	0.172	0.396	0.088	0.061	0.083	0.026	0.022	6.587	4.84
GI- 30	0.455	0.148	0.252	0.023	0.035	0.062	n.d.	0.025	3.152	3.26

n.d. = not detected.

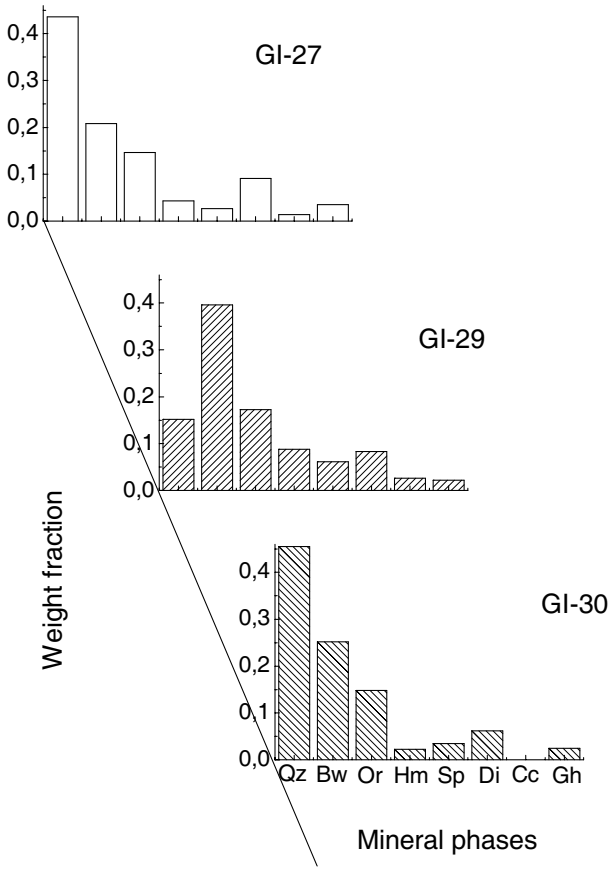

Fig. 9. – Histogram plot of phase fractions for the analysed samples: Qz, quartz, Bw, bytownite, Or, orthoclase; Hm, haematite; Sp, spinel; Di, diopside; Cc, calcite; Gh, gehlenite.

GI-29, that exhibits a different behaviour. In particular, GI-29 reveals, if compared to GI-27 and GI-30, a very low quartz percentage and higher amounts of bytownite, haematite and spinel.

Again, as already attested by INAA and FT-IR absorbance, since any correlation with the firing process can be inferred, these quantitative variations should be attributed to raw minerals extracted from different quarries.

4. – Conclusions

In the present work, a set of four ancient pottery shards was investigated. The samples, finely decorated with red figures, come from the archaeological site of Gioiosa Guardia (Sicily) and are dated back to VI-V century b. C. The complementary application of several experimental microdestructive, such as INAA and FT-IR absorbance, and non-destructive, such as TOF-ND, techniques allowed for a detailed characterization of the findings.

Despite the low statistics due to the small number of the analysed fragments, the trace element analysis, performed by INAA, allowed us to classify the findings into two

sub-groups: on one side, GI-27 and GI-30 show Cr and Ni contents typical of the Greek productions, whereas, on the other side, GI-28 and GI-29 exhibit values representative for Western productions. Of course, this classification has to be considered only as a kind of example that could be more meaningfully applied when a larger number of samples are available.

FT-IR absorbance and TOF-ND techniques allowed, respectively, the qualitative and quantitative determination of the main phases in this type of pottery, revealing the mineralogical compositions of the samples.

The differences revealed in the mineralogical composition confirmed the grouping of the shards hypothesized by INAA, suggesting differences concerning the origin of the potteries of each sub-group.

For all the analysed samples, the firing temperature was estimated to be in the range of 900–950 °C. In addition, FT-IR results revealed a higher amount of clay and iron oxides on the samples surface with respect to the inner bulk, thus validating the application of the typical Greek red-figures decoration process.

Starting from the obtained information, a classification and cataloguing of the ancient findings can be achieved. In addition, when used in combination with results from other archaeometric methods, the present data can be very useful in order to formulate hypotheses concerning the provenance of the pottery.

* * *

This research has been financially supported by the PRIN2007.

REFERENCES

[1] Cogswell J. W., Neff H. and Glacock M. D., *J. Archaeol. Sci.*, **23** (1996) 283.
[2] Day P. M., Kiriatzi E., Tsolakidou A. and Kilikoglou V., *J. Archaeol. Sci.*, **26** (1999) 1025.
[3] Barilaro D., Crupi V., Majolino D., Venuti V., Barone G. and Kockelmann W., *J. Appl. Phys.*, **98** (2005) 103520.
[4] Barilaro D., Crupi V., Majolino D., Venuti V., Barone G. and Kockelmann W., *J. Archaeol. Sci.*, **34** (2007) 1148.
[5] Siouris I. M. and Walter J., *Phys. B*, **385-386** (2006) 225.
[6] Sondi I. and Slovenec D., *Archaeom.*, **45** (2003) 251.
[7] Botti A., Ricci M. A., De Rossi G., Kockelmann W. and Sodo A., *J. Archaeol. Sci.*, **33** (2006) 307.
[8] Triolo R., Lo Celso F., Benfante V., Gorgoni C., Barker J., Butler P. and Ruffo I., *Nuovo Cimento C*, **30** (2007) 129.
[9] Jordan S. C., Schrire C. and Miller D., *J. Archaeol. Sci.*, **26** (1999) 1327.
[10] Buxeda J., Garrigós I., Cau Ontiveros M. A. and Kilikoglou V., *Archaeom.*, **45** (2007) 1.
[11] Buxeda J., Garrigós I., Jones R. E., Kilikoglou V., Levi S. T., Maniatis Y., Mitchell J., Vagnetti L., Wardle K. A. and Andreou S., *Archaeom.*, **45** (2003) 263.
[12] Pierret A., Moran C. J. and Bresson L. M., *J. Archaeol. Sci.*, **23** (1996) 419.
[13] Kockelmann W., Kirfel A., Siano S. and Frost C. D., *Phys. Ed.*, **39** (2004) 155.
[14] Lindstrom R. M. and Yonezawa C., in *Prompt Gamma Neutron Activation Analysis* (CRC Press, Boca Raton, FL) 1995, p. 93.
[15] Schillinger B., Lehmann E. and Vontobel P., *Phys. B*, **276-278** (2000) 59.
[16] Kardjilov N., Lo Celso F., Donato D. I., Hilger A. and Triolo R., *Nuovo Cimento C*, **30** (2007) 79.

[17] Kockelmann W., Pantos E. and Kirfel A., in *Radiation in Art and Archaeometry* (Elsevier, Amsterdam) 2000, p. 347.
[18] Kockelmann W., Kirfel A. and Hähnel E., *J. Archaeol. Sci.*, **28** (2001) 213.
[19] Kockelmann W., Weißer M., Heinen H., Kirfel A. and Schäfer W., *Mater. Sci. Forum*, **321-324** (2000) 332.
[20] Siano S., Kockelmann W., Bafile U., Celli M., Pini R., Salimbeni R., Iozzo M., Miccio M., Moze O. and Zoppi M., *Appl. Phys. A*, **74** (2002) S1139.
[21] Artioli G., Kockelmann W., Magerl A., Mezei F., Rinaldi R., Schäfer W., Schofield P. F. and Zoppi M., in *Cultural Heritage: Artefacts and Materials II* (The ESS Project, ESS Council) 2002, pp. 6-54.
[22] Wenk H.-R. and Van Houtte P., *Rep. Prog. Phys.*, **67** (2004) 1367.
[23] Artioli G., Dugnani M., Angelini I., Lutterotti L., Pedrotti A. and Fleckinger A., *Proc. Archaeometall. Eur.*, **2** (2003) 9.
[24] Pantos E., Kockelmann W., Chapon L. C., Lutterotti L., Bennet S. L., Tobin M. J., Mosselmans J. F. W., Pradell T., Salvado N., Butì S., Garner R. and Prag A. J. N. W., *Nucl. Instrum. Methods B*, **239** (2005) 16.
[25] Kockelmann W., Kirfel A., Jansen E., Linke R., Schreiner M., Traum R. and Denk R., *Proceedings Numismatics & Technology* (Kunsthistorisches Museum Wien) 2003, p. 113.
[26] Kockelmann W., Siano S., Bartoli L., Visser D., Hallebeek P., Traum R., Linke R., Schreiner M. and Kirfel A., *Appl. Phys. A*, **83** (2006) 175.
[27] Voza G., in *Gioiosa Vecchia, BCA Sicilia anno III*, n. 1-2-3-4 (1982).
[28] Albanese Procelli R. M., in *Sicani, Siculi, Elimi, Forme di Identità, Modi di Contatto e Processi di Trasformazione* (Longanesi & C., Milano) 2003.
[29] Glascock M. D. and Neff H., *Meas. Sci. Technol.*, **14** (2003) 1516.
[30] *Sadtler IR database, Minerals and Clays* (Bio-Rad Laboratories) 1998.
[31] Willis B. T. M., *Z. Kristall.*, **209** (1994) 385.
[32] Larson A. C. and VonDreele R. B., in *GSAS: General Structure Analysis Software* (`www.ccp14.ac.uk`).
[33] Young R. A., in *The Rietveld Method* (Oxford University Press, New York) 1993.
[34] Barone G., Ioppolo S., Majolino D., Migliardo P. and Tigano G., *J. Cult. Herit.*, **3** (2002) 145.
[35] Capel J., Huertas F. and Linares J., in *Miner. Petrogr. Acta*, **29** (1985) 563.
[36] Duminuco P., Riccardi M. P., Messiga B. and Setti M., *Ceramurgia*, **5** (1996) 281.
[37] *ICSD, Inorganic Crystal Structure Database*, Fachinformationszentrum *Karlsruhe*, National Institute of Standards and Technology, USA (1999).